JOC The Journal of Organic Chemistry

Article

pubs.acs.org/joc

Supramolecular Gelation of Rigid Triangular Macrocycles through Rings of Multiple C−H···O Interactions Acting Cooperatively

Zhichang Liu,[†] Junling Sun,[†] Yu Zhou,[‡] Yu Zhang,[†,§] Yilei Wu,[†] Siva Krishna Mohan Nalluri,[†] Yuping Wang,[†] Avik Samanta,[†] Chad A. Mirkin,[†,‡] George C. Schatz,[†,§] and J. Fraser Stoddart*[,†]

[†]Department of Chemistry, Northwestern University, 2145 Sheridan Road, Evanston, Illinois 60208-3113, United States

[‡]Department of Materials Science and Engineering, Northwestern University, 2220 Campus Drive, Evanston, Illinois 60208-3113, United States

[§]Center for Bio-inspired Energy Science, Northwestern University, 2145 Sheridan Road, Evanston, Illinois 60208-3113, United States

Supporting Information

ABSTRACT: When equimolar solutions of the enantiomeric naphthalenediimide-based highly rigid triangles ***R*-Δ** and ***S*-Δ** in $ClCH_2CH_2Cl$ are mixed, the racemate ***rac*-Δ** forms an organogel that is composed of interwoven fibers, resulting from the columnar stacking of the triangles in an alternating ***R*-Δ**/***S*-Δ** fashion. Under identical conditions, the pure enantiomers do not form organogels. Density functional theory calculations reveal that the racemic *RS* dimer is more stable than the *RR* dimer as a result of the enantiomeric relationship between ***R*-Δ** and ***S*-Δ**, allowing them to act as two complementary rings comprised of 12 [C−H···O] interactions with an unprecedented and uninterrupted circular ADDAADDAADDA·DAADDAADDAAD alignment of hydrogen bond donors (D) and acceptors (A), in contrast with the square-wave manner in which the *RR* dimer forms a complementary yet interrupted ADADAD·DADADA circular sequence of six longer [C−H···O] hydrogen bonds. It follows that gelation is favored by weak interactions acting cooperatively in rings under precise stereoelectronic control.

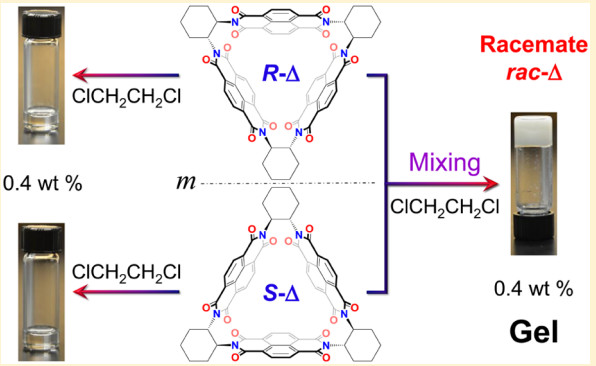

INTRODUCTION

Low-molecular weight gelators (LMWGs) are capable of assembling into interwoven fibrillar networks that entrap solvents between strands to form thermoreversible supramolecular gels.[1−10] Chirality[11−13] has a profound influence on the macroscopic gelation of solvents by facilitating the growth and stabilization of noncovalent helical fibers as well as their interwoven networks, often driven by stereogenic centers present in the molecular structures of chiral LMWGs. As a consequence, most of the highly efficient LMWGs, exhibiting strong gelling ability, are[1,14−16] composed of enantiomerically pure chiral molecules. In general terms, the corresponding racemates of these enantiopure chiral gelators either do not form gels or occasionally form only weak ones that transform readily into precipitates or discrete crystals.[12,17,18] The opposite situation, in which a racemate generates a gel, while both its enantiomers are less efficient gelators, or even lack any gelling ability at all, is rare. Although there are a few examples[18−26] of gels resulting from the assembly of racemic gelators incorporating flexible structures, driven by means of various noncovalent bonding interactions, gels assembled from highly rigid racemic gelators at the behest of multiple weak [C−H···O] interactions[27] as the major driving force remain unexplored to the best of our knowledge. Kim et al.[28] have reported that rigid achiral cucurbit[7]uril (CB[7]) can act as a hydrogelator, but only in the presence of mineral acids. The relationship between stereochemistry and gelation, however, has yet to be fully elucidated.

Hydrogen-bonding arrays are well-established modules for the formation of biotic[29] and abiotic[30] supramolecular polymers, as well as for the assembly of cylindrical[31−33] and spherical[34−36] capsules. While a number of planar quadruple hydrogen-bonding motifs give rise[37−40] to supramolecular arrays, cyclic peptides are among the few well-known examples of multiple hydrogen-bonding ring motifs that lead[41−43] to the formation of supramolecular nanotubes. Also, despite the remarkable progress that has been made in recent years, interactions involving hydrogen-bonding motifs have been restricted for the most part to the use of [O−H···O][44,45] and [N−H···O][29,30,41,46−49] noncovalent bonds because of their greater strengths and propensities to act cooperatively. These strong noncovalent bonds facilitate the construction of well-defined supramolecular assemblies by overriding the influence of other competing interactions from mismatched molecular structures, counterions, and solvents. Permutations of hydrogen

Received: February 10, 2016
Published: February 26, 2016

DOI: 10.1021/acs.joc.6b00281
J. Org. Chem. 2016, 81, 2581−2588

bonds composed of multiple intermolecular cooperative [C−H···O] interactions,[49] leading to the formation of supramolecular assemblies, have remained largely out of reach because of the relative weakness of single [C−H···O] interactions. We have found, however, that employing these weak interactions cooperatively as the major driving force to create supramolecular assemblies becomes a real possibility when the multiple [C−H···O] hydrogen bonds are arranged in rings.

Herein, we report an example of circular [C−H···O] interaction-driven supramolecular gelation that occurs (Figure 1a) upon mixing equimolar amounts of the enantiomeric

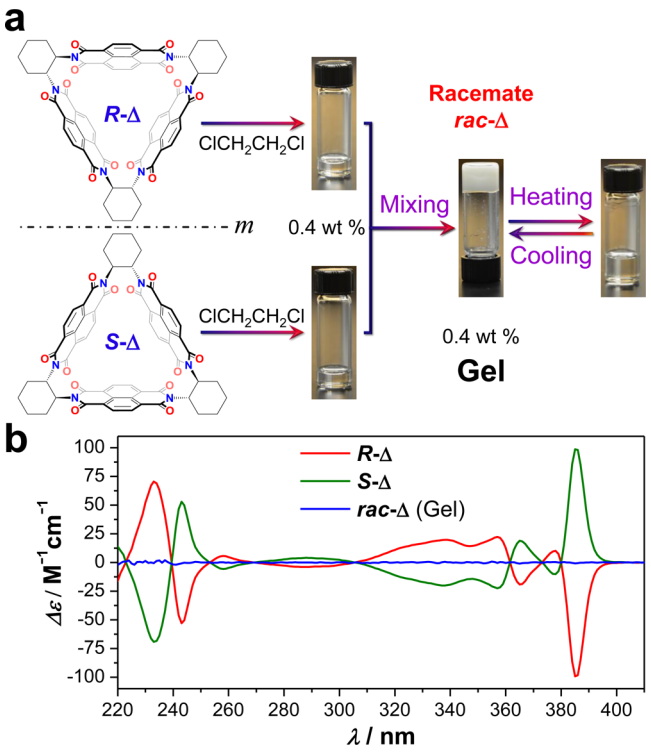

Figure 1. Gelation of the racemate from equimolar amounts of ***R*-Δ** and ***S*-Δ** together with CD analyses. (a) Structural formulas of ***R*-Δ** and ***S*-Δ**, followed by photographs of the formation of thermoreversible gels from the racemate ***rac*-Δ** by mixing ***R*-Δ** and ***S*-Δ** in $ClCH_2CH_2Cl$ at a 1:1 molar ratio at concentrations of 0.4 wt %. (b) CD spectra of ***R*-Δ** and ***S*-Δ** in addition to the redissolved racemate ***rac*-Δ**, which is obtained by centrifugation of the gel, in $ClCH_2CH_2Cl$.

naphthalenediimide-based rigid triangular macrocycles (NDI-Δ), namely, ***R*-Δ** and ***S*-Δ**.[51,52] It relies on the formation of one-dimensional (1D) fibers brought about by the coaxial stacking assembly of ***R*-Δ** and ***S*-Δ** in an alternating fashion, driven predominantly by rings of multiple weak [C−H···O] interactions acting cooperatively at the interfaces between ***R*-Δ** and ***S*-Δ**. Density functional theory (DFT) calculations reveal that the energetically more favorable stereochemical match between ***R*-Δ** and ***S*-Δ** allows them to act as two complementary double-faced 12-point [C−H···O] hydrogen-bonded circular arrays with an unprecedented and uninterrupted ADDAADDAADDA·DAADDAADDAAD hydrogen-bonding sequence. As a consequence, this strategy reinforces the strength and facilitates the cooperativity and linear directionality of 12 circular [C−H···O] interactions between ***R*-Δ** and ***S*-Δ** to drive the 1D supramolecular assembly of the racemate ***rac*-Δ** of ***R*-Δ** and ***S*-Δ** to form organogels.

RESULTS AND DISCUSSION

Gelation of *rac*-Δ. When equimolar solutions of ***R*-Δ** and ***S*-Δ** in $ClCH_2CH_2Cl$ (DCE) are mixed together, a self-supporting gel is formed (Figure 1a) with the racemate ***rac*-Δ** as a gelator within minutes. It should be emphasized that, despite the fact that the solubilities of enantiopure ***R*-Δ** and ***S*-Δ** are at least as high as 20 g/L in DCE, mixing two equimolar solutions (5 g/L, 0.4 wt %) of ***R*-Δ** and ***S*-Δ** in DCE results, nonetheless, in the gelation of the mixture as evidenced by a homogeneous solidlike material that exhibits no gravitational flow whatsoever. Upon being heated, the gel (0.4 wt %) transforms into a clear solution with a melting temperature of 69−73 °C, which resorts on cooling to forming a gel, confirming its thermoreversibility. In addition, this gel has also been made by dissolving a racemate of solid ***R*-Δ** and ***S*-Δ** in DCE directly by heating, followed by cooling the mixture to ambient temperature. In contrast to the strong mirror-symmetrical circular dichroism (CD) responses of enantiopure ***R*-Δ** and ***S*-Δ**, the silent CD signal of a redissolved sample prepared from the centrifuged gel confirms (Figure 1b) its racemic nature.

In view of the unexpected gelation of the racemate ***rac*-Δ** in DCE, the gelation abilities of ***rac*-Δ** in three 1,2-dihaloethanes (DXEs) as well as CH_2Cl_2 and $CHCl_3$ were also assessed (Table 1). Enantiopure ***R*-Δ** and ***S*-Δ** are soluble in all of these

Table 1. Solvent-Dependent Gelation Behavior of *R*-Δ and *S*-Δ as Well as *rac*-Δ[a]

solvent	***R*-Δ** or ***S*-Δ**	***rac*-Δ**
CH_2Cl_2	solution	precipitate
$CHCl_3$	solution	precipitate
$ClCH_2CH_2Cl$	solution	gel
$ClCH_2CH_2Br$	solution	precipitate
$ClCH_2CH_2I$	solution	precipitate
$BrCH_2CH_2Br$	solution	precipitate

[a]All experiments were conducted at the same concentration of 0.4 wt %.

solvents at the same concentration of 0.4 wt % under similar conditions. In striking contrast, when equal volumes of 0.4 wt % solutions of ***R*-Δ** and ***S*-Δ** in these solvents are mixed, three different types of aggregates are observed: (i) a self-supporting thermoreversible organogel that formed in DCE, (ii) white fibrous precipitates that appeared in $ClCH_2CH_2Br$ (CBE), $ClCH_2CH_2I$ (CIE), and $BrCH_2CH_2Br$ (DBE) within 10 min, and (iii) white flocculent precipitates that emerged after ∼10 min in CH_2Cl_2 and $CHCl_3$. The morphologies of these different aggregated states of ***rac*-Δ** were probed by scanning electron microscopy (SEM).

SEM analysis of ***rac*-Δ** in DCE revealed (Figure 2a) that the organogel is formed by an interwoven fibrillar network, composed of high-aspect ratio flexible fibers with lengths on the order of several hundred micrometers and diameters on the order of several hundred nanometers. The precipitate of ***rac*-Δ** in DBE has been characterized (Figure 2b) as forming high-aspect ratio, but more rigid, as well as thicker and straight needles, which exercise their ability to generate an entangled network. This observation indicates that both the gel and the precipitate of ***rac*-Δ** in DCE and DBE, respectively, are

DOI: 10.1021/acs.joc.6b00281
J. Org. Chem. 2016, 81, 2581−2588

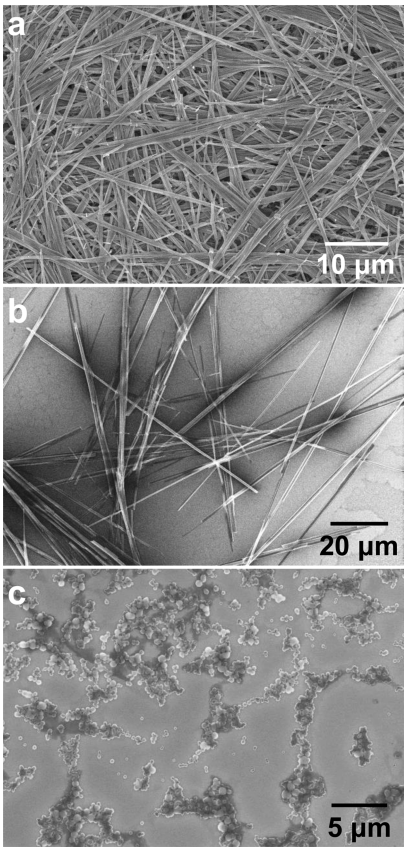

Figure 2. Morphologies of samples of ***rac*-Δ** in different solvents spin-coated on silicon wafers as observed by SEM. (a) Interwoven fibrillar network from the gel of ***rac*-Δ** in $ClCH_2CH_2Cl$. (b) Discrete needles from a precipitate of ***rac*-Δ** in $BrCH_2CH_2Br$. (c) Random-shaped aggregates from a precipitate of ***rac*-Δ** in $CHCl_3$.

generated by means of a similar mechanism[52] involving the formation of high-aspect ratio 1D fibers as a result of cooperative action of the [X···X]-bonded DXE chains inside the NDI-Δ supramolecular nanotubes. Good cooperation between the weaker [Cl···Cl] interactions and the shorter length of DCE (4.33 Å), compared with the stronger [Cl···Br], [Cl···I], and [Br···Br] interactions as well as the longer lengths exhibited in CBE (4.48 Å), CIE (4.68 Å), and DBE (4.62 Å), give[52] rise to a more dense network of fibers that facilitates the gelation of ***rac*-Δ** in DCE involving the formation of the entangled fibrous network. By contrast, SEM images of the flocks of ***rac*-Δ** in $CHCl_3$ show (Figure 2c) random-shaped aggregates with variable diameters in size, suggesting that ***rac*-Δ** might be unable to stack unidirectionally, forming 1D fibers over a long range because of the lack[52] of the templating effect of the shorter constitution associated with $CHCl_3$. The 1D fibers formed from ***rac*-Δ** in DCE and DBE were also investigated by powder X-ray diffraction (PXRD). Both PXRD patterns (Figure S1) for the vacuum-evacuated gel of ***rac*-Δ** in DCE and precipitate of ***rac*-Δ** in DBE resemble one another closely. The sharper diffraction peaks observed for the precipitate of ***rac*-Δ** in DBE are in line with the better rigidity and crystallinity of the 1D fibers formed from ***rac*-Δ** in DBE than that in DCE. These observations, in combination with our previous conclusion[52] that 1D supramolecular nanotubes form only from ***R*-Δ** or ***S*-Δ** in DXEs, (i) confirm the similar packing motifs of the 1D high-aspect ratio fibers, formed from ***rac*-Δ** in DCE and DBE, and (ii) provide strong evidence of the same assembly mechanism of 1D fibers through columnar stacking of ***rac*-Δ** with the assistance of the templating effect of the [X···X]-bonded DXE chains.

Oscillatory rheology that was performed to characterize the mechanical properties of the organogel (1.0 wt % ***rac*-Δ** in DCE) revealed (Figure 3) that the storage modulus G' is 20

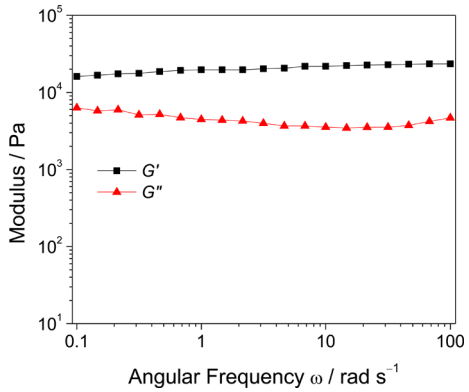

Figure 3. Frequency sweep (0.02% strain) rheological measurements for the organogel of 1.0 wt % ***rac*-Δ** in $ClCH_2CH_2Cl$ at 25 °C. G' is the storage modulus; G'' is the loss modulus.

kPa, which is greater than the corresponding loss modulus G'' of 4 kPa. It is worth noting that the example of such a fully rigid macrocycle acting as a gelator at a concentration as low as 0.4 wt % without any additives except for the solvent is unprecedented to the best of our knowledge. In contrast, ***rac*-Δ** in CBE, CIE, and DBE produces more rigid high-aspect ratio fibers that are unable to form self-supporting gels through entangling to afford networks, leading to precipitation.

Atomic Force Microscopy (AFM) Analyses. To gain insight into the initial assembly mechanism of the high-aspect ratio fibers of ***rac*-Δ** in DCE and DBE, AFM was performed on them. Two samples were prepared by spin-coating both dilute clear solutions (0.5 g/L) of ***rac*-Δ** in DCE and DBE onto mica surfaces. The sample of ***rac*-Δ** in DCE reveals (Figure 4a) discrete thin micrometer-long nanofibers with diameters of ∼10 nm, which we believe are composed of a bundle of ∼2.2 nm diameter supramolecular nanotubes formed (Figure 4c) from the columnar stacking of alternate ***R*-Δ** and ***S*-Δ** with a 60° rotational angle. The AFM image of the sample of ***rac*-Δ** in DBE shows (Figure 4b) high-aspect ratio nanotubes with lengths on the order of several micrometers. Cross-section analysis indicates unambiguously that these nanotubes have a height of 2.4 ± 0.4 nm, a dimension that corresponds well with the outer diameter of ∼2.2 nm of the proposed ***R*-Δ** and ***S*-Δ** stacking in an alternating fashion to form (Figure 4c) supramolecular nanotubes. This level of consistency confirms the fact that ***rac*-Δ** assembles into single supramolecular nanotubes with aspect ratios as high as ≥1000 as a result of the columnar stacking of ***rac*-Δ** in which ***R*-Δ** and ***S*-Δ** are positioned in a 60° rotationally alternating manner. In addition, several single-molecule-scale nanotubes aggregate in parallel at long range, suggesting that the high-aspect ratio fibers observed in the SEM sample of ***rac*-Δ** in DBE could be assembled from a bundle of supramolecular nanotubes with diameters of ∼2.2 nm. Considering the closely similar PXRD patterns (Figure S1) of the gel of ***rac*-Δ** in DCE and the precipitate of ***rac*-Δ** in DBE, the formation of thicker nanofibers in the case of ***rac*-Δ** in DCE is comparable with that in DBE. The nanofibers are believed to

DOI: 10.1021/acs.joc.6b00281
J. Org. Chem. 2016, 81, 2581−2588

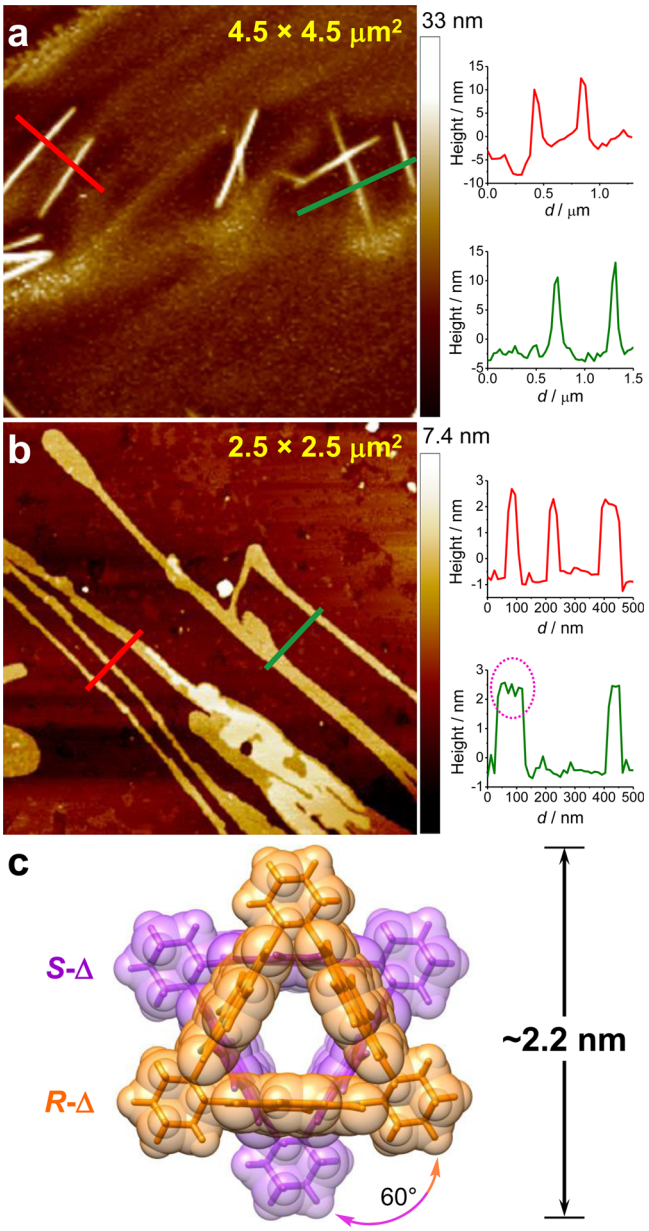

Figure 4. AFM images and topographical analyses. The height sensor images of (a) a sample of ***rac*-Δ** in $ClCH_2CH_2Cl$ and (b) a sample of ***rac*-Δ** in $BrCH_2CH_2Br$ spin-coated on mica, in addition to the corresponding cross-sectional analysis of the nanofibers. The line colors in the height images correspond to the line colors of the profile plots. The magenta circle in panel b highlights the profile of parallel aggregated nanofibers. (c) Space-filling overlying a tubular representation of the top view of the columnar stacked dimer of ***R*-Δ** and ***S*-Δ** with a 60° rotational angle between them and an outer diameter of ~2.2 nm.

originate from the parallel packing of single-molecule-scale supramolecular nanotubes as a consequence of the rapid volatilization of low-boiling point DCE during the spin-coating process. The observation of high-aspect ratio supramolecular nanotubes with diameters on the single-molecule scale also indicates that the axial noncovalent bonding interactions—namely, [C−H···O] and [X···X] between DXE molecules inside the nanotubes—play a defining role in directing and driving the highly efficient formation of these 1D assemblies.

Density Functional Theory (DFT) Calculations. In an attempt to understand why the racemate ***rac*-Δ** forms gels and precipitates while the pure enantiomers ***R*-Δ** and ***S*-Δ** do not, we investigated these systems by quantum chemical calculations [Q-Chem 4.2.0/PBE/6-311G** (see the Supporting Information)]. As models, we studied two representative systems, that is, a racemic *RS* dimer and an enantiopure *RR* dimer composed (Figure 5a,b) of columnarly stacked ***R*-Δ** and ***S*-Δ** or two ***R*-Δ**s, respectively. DFT optimization results revealed (Figure 2 and Figure S2) that the *RS* dimer has a binding energy (ΔG) of −34.5 kcal mol^{-1}, whereas the *RR* dimer has a ΔG value of −32.7 kcal mol^{-1}. It follows that the *RS* dimer is 1.8 kcal mol^{-1} more stable than the *RR* dimer on the basis of the same energies considered for ***R*-Δ** and ***S*-Δ**, an observation that suggests that the aggregates of ***rac*-Δ** should be thermodynamically more stable than those of either ***R*-Δ** or ***S*-Δ** and thus is in good agreement with the observed experimental results (Figure 2) for the formation of the aggregates of ***rac*-Δ** while ***R*-Δ** remains in solution. The binding energy difference of 1.8 kcal mol^{-1} equates well with the modest melting temperature (69−73 °C) of the gel. Geometrical analysis revealed (Figure 5a,b) that (i) the two NDI-Δs in the *RS* dimer are 0.04 Å closer than in the *RR* dimer and (ii) the rotational angle between two NDI-Δs in the *RS* dimer is 60°, giving rise to the C_3 symmetry of the *RS* dimer, whereas the angle in the *RR* dimer is 65° with a 5° deviation from C_3 symmetry. These observations suggest two possibilities: (i) the [C−H···O] hydrogen bonding interactions between ***R*-Δ** and ***S*-Δ** are stronger than those between two ***R*-Δ**s; (ii) the columnar stacking of the *RS* dimer leads to nonhelical supramolecular nanotubes, while that of the *RR* dimer results in helical ones as shown previously.[52] The [C−H···O] hydrogen bonding patterns of both dimers are depicted in panels c and d of Figure 5, wherein the diastereotopic NDI protons are designated as H_a and H_b, the corresponding C atoms of which are termed C_a and C_b, respectively. Analysis of [C−H···O] interaction distances ($d_{C\cdots O}$) reveals (Figure 5e,f and Table S1) that in both dimers, all $d_{Cb\cdots O}$ values are much greater than all $d_{Ca\cdots O}$ values. All $d_{Ca\cdots O}$ values in both dimers are very close with a mean $d_{Ca\cdots O}$ of 3.15 Å (mean $\angle C_a{-}H_a\cdots O$ of 152.1°) for the *RS* dimer and one of 3.13 Å (mean $\angle C_a{-}H_a\cdots O$ of 161°) for the *RR* dimer, suggesting that all the H_a atoms form strong [$C_a{-}H_a\cdots O$] hydrogen bonds with imide O atoms. By contrast, a mean $d_{Cb\cdots O}$ of 3.45 Å (mean $\angle C_b{-}H_b\cdots O$ of 161.8°) in the *RS* dimer is 0.1 Å shorter than that of 3.55 Å (mean $\angle C_b{-}H_b\cdots O$ of 152.3°) in the *RR* dimer, an all but negligible value to be considered as a [C−H···O] interaction,[53] indicating that there are modest [$C_b{-}H_b\cdots O$] interactions in the *RS* dimer, whereas [$C_b{-}H_b\cdots O$] interactions in the *RR* dimer are nonexistent. In the case of the *RS* dimer, [$C_a{-}H_a\cdots O$] and [$C_b{-}H_b\cdots O$] hydrogen bonds are alternatingly arranged (Figure 5e) in a triangular wave with an unprecedented and uninterrupted complementary 12-point ADDAADDAADDA·DAADDAADDAAD hydrogen-bonding sequence, while in the case of the *RR* dimer, [$C_a{-}H_a\cdots O$] and [$C_b{-}H_b\cdots O$] hydrogen bonds are doubly alternatingly arranged (Figure 5f) in a square-wave manner with a complementary six-point ADADAD·DADADA hydrogen bonding sequence because of the weakness of the [$C_b{-}H_b\cdots O$] hydrogen bonds. The stronger [$C_b{-}H_b\cdots O$] hydrogen bonds, which are in good agreement with the shorter distance between two NDI-Δs and the lower energy of the *RS* dimer, in cooperation with the more even arrangement of alternating strong and weak hydrogen bonds, endow ***rac*-Δ** with a stronger

DOI: 10.1021/acs.joc.6b00281
J. Org. Chem. 2016, 81, 2581−2588

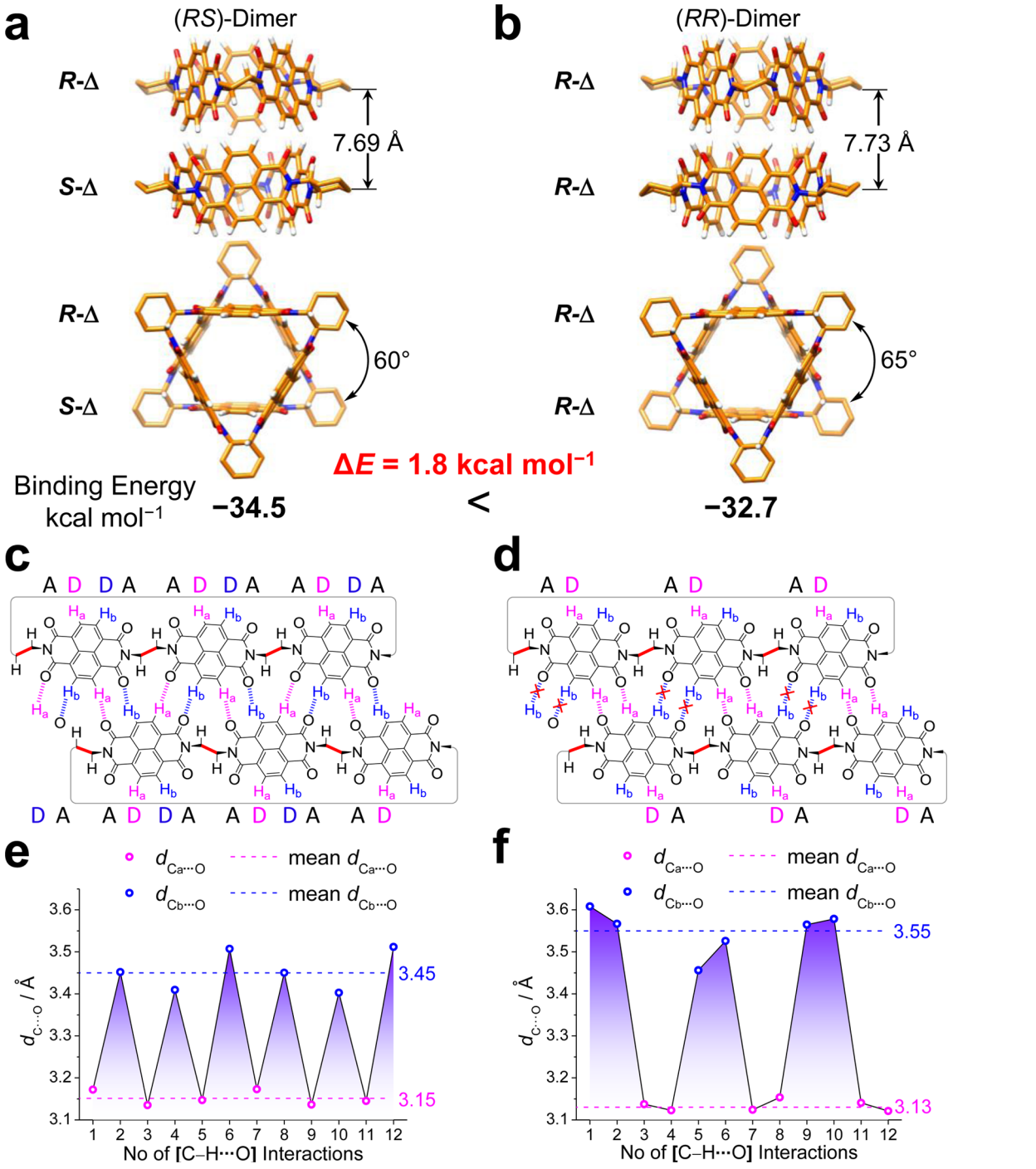

Figure 5. Results of DFT calculations. (a and b) Side-on and top views of stick models showing the relative orientations of ***R*-Δ** and ***S*-Δ** in the optimized superstructures of the *RS* dimer and *RR* dimer, respectively. C atoms are colored orange, H atoms white, O atoms red, and N atoms blue. Hydrogen atoms on achiral carbon atoms of 1,2-cyclohexano rings have been omitted for the sake of clarity. (c and d) Schematic views of the [C–H···O] interactions (magenta hatched lines) between two NDI-Δ macrocycles of the *RS* dimer and the *RR* dimer, respectively, as well as the relative positions of the diastereotopic NDI protons H_a (*cis*, magenta) and H_b (*trans*, blue) to the adjacent protons on the stereogenic center of the 1,2-cyclohexano rings (bold red bonds). [C_a–H_a···O] and [C_b–H_b···O] hydrogen bonds are depicted as magenta and blue hatched lines, respectively. A and D indicate hydrogen bonding acceptors and donors, respectively. Red crosses indicate nonexistent [C–H···O] hydrogen bonds for which $d_{C\cdots O}$ > 3.5 Å. (e and f) Analysis of $d_{C\cdots O}$ of [C–H···O] interactions between two NDI-Δ macrocycles of the *RS* dimer and the *RR* dimer, respectively.

ability to aggregate giving fibers, whereas neither ***R*-Δ** nor ***S*-Δ** can form similar aggregates under the same conditions because of the less stable noncovalent bonding interactions, resulting from the inferior stereochemical match between two ***R*-Δ**s or ***S*-Δ**s. These observations, taken together, suggest that the energetically more favorable match between ***R*-Δ** and ***S*-Δ** allows them to act as two unique double-faced 12-point [C–H···O] hydrogen-bonded rings that can enhance the cooperativity[54] and directionality of the hydrogen bonds, resulting in the 1D supramolecular assembly[55] of ***rac*-Δ**. Although strong [O–H···O],[44,45] [N–H···O],[29,30,41,46−49] π–π stacking,[47,56−59] and ion-pairing[60,61] interactions, as well as weak halogen

DOI: 10.1021/acs.joc.6b00281
J. Org. Chem. 2016, 81, 2581−2588

bonding[62] and [C−H···π][63] interactions, have been employed oftentimes in supramolecular polymerizations, related examples facilitated predominantly by multiple weak [C−H···O] interactions[64,65] acting circularly and cooperatively have not, to the best of our knowledge, been explored.

^{1}H and Two-Dimensional (2D) DOSY NMR Analyses. To probe the influence of different strengths of [C−H···O] interactions between ***R*-Δ** and ***S*-Δ** as well as enantiopure ***R*-Δ** on the chemical shifts of the diastereotopic NDI protons H_a and H_b, variable-temperature (VT) ^{1}H NMR spectroscopy was conducted. All VT ^{1}H NMR spectra of ***rac*-Δ** and ***R*-Δ** recorded in $ClCD_2CD_2Cl$ [−30 to 80 °C (Figure S3)], $BrCD_2CD_2Br$ [10−110 °C (Figure S4)], and $CDCl_3$ [−30 to 60 °C (Figure S5)] at the same concentration show similar trends with no significant differences between the changes in chemical shifts of H_a and H_b of both ***rac*-Δ** and ***R*-Δ**. This observation indicates that the weak nature of [C−H···O] interactions might not be enough to lead to the ^{1}H NMR-detectable difference in the chemical environments between ***rac*-Δ** and ***R*-Δ**, even if the [C−H···O] interactions between ***R*-Δ** and ***S*-Δ** are stronger than those between two ***R*-Δ**s as supported by DFT calculations. DOSY NMR experiments were performed to investigate the aggregation behaviors of ***rac*-Δ** and ***R*-Δ** in the solution phase. DOSY NMR spectra of both ***rac*-Δ** and ***R*-Δ** in $ClCD_2CD_2Cl$ (Figure S6), $BrCD_2CD_2Br$ (Figure S7), and $CDCl_3$ (Figure S8), analyzed under the same conditions, give very similar diffusion coefficients (D). For example, although flocks already appeared in solutions of ***rac*-Δ**, those of ***R*-Δ** are still clear at −30 °C at a concentration of 0.6 g/L in $ClCD_2CD_2Cl$, and D values of ***rac*-Δ** and ***R*-Δ** are measured to be 0.82×10^{-10} and 0.84×10^{-10} m^2 s^{-1}, respectively. These observations suggest that the gelation and precipitation of ***rac*-Δ**, in contrast with that of enantiopure ***R*-Δ** or ***S*-Δ**, might be the result of a cooperative mechanism facilitated by the subtle interplay between [C−H···O] interactions and better matched steric configurations of ***R*-Δ** and ***S*-Δ**, which is not detectable on the ^{1}H NMR time scale by DOSY experiments presumably because of the rapid dynamic exchange of species in solution.

CONCLUSIONS

In summary, we have demonstrated that equimolar mixing of ***R*-Δ** and ***S*-Δ** leads to the assembly of ***rac*-Δ** into a supramolecular gel composed of entangled fibrillar networks in DCE, whereas neither enantiopure ***R*-Δ** nor enantiopure ***S*-Δ** forms fibrous aggregates under identical conditions. These organogels are comprised of fibers, produced by the columnar stacking of alternate ***R*-Δ** and ***S*-Δ** and driven synergistically by rings of 12 weak [C−H···O] hydrogen bonds in a circular manner, assisted by a good match between the ***R*-Δ** and ***S*-Δ** enantiomers. DFT calculations testify to the fact that the *RS* dimer is 1.8 kcal mol^{-1} more stable than the *RR* dimer and that the [C−H···O] interactions between ***R*-Δ** and ***S*-Δ** are much stronger and more cooperative than those between two ***R*-Δ**s or ***S*-Δ**s. These experimental results, in conjunction with DFT calculations, provide and account for this example of supramolecular gelation from rigid racemic gelators, rather than their enantiopure counterparts, an observation that highlights the fundamental relationship between stereochemistry and gelation. The use of the multiple weak [C−H···O] interactions acting cooperatively in rings to provide the major driving force represents a promising design strategy for LMWGs that relies on the subtle interplay between stereochemistry and weak noncovalent bonding interactions, expanding the scope of LMWGs to rigid racemates in the absence of strong hydrogen-bonded motifs and flexible structures. The fact that many organic compounds contain (C−)H atoms and C═O groups (or O atoms) that can play the roles of hydrogen bond donors and acceptors, respectively, means that intramolecular arrays with intermolecular stereoelectronic matches of multiple [C−H···O] interactions can, in principle, act cooperatively in a supramolecular context to produce a wide variety of new soft materials.

EXPERIMENTAL SECTION

General. All reagents were purchased and used without further purification. The macrocyclic triangles ***R*-Δ** and ***S*-Δ** were synthesized as described previously.[51] Variable-temperature ^{1}H and 2D DOSY NMR spectra were recorded on a NMR spectrometer with a working frequency of 500 MHz for ^{1}H. Chemical shifts are reported in parts per million relative to the signals corresponding to the residual nondeuterated solvents ($CDCl_3$, δ 7.26; $ClCD_2CD_2Cl$, δ 3.72; $BrCD_2CD_2Br$, δ 3.63). Circular dichroism (CD) measurements were taken on a CD spectrometer, and the HT voltage was maintained below 600 V.

Preparation and Characterization of Organogels and Precipitates. Gel and precipitate formations were conducted by mixing equal volumes of solutions of both ***R*-Δ** and ***S*-Δ** in vials at the same concentration of 0.4 wt %. The gels can also be made by directly dissolving the racemate ***rac*-Δ** as a solid in $ClCH_2CH_2Cl$ (DCE) by heating, followed by cooling the mixture to ambient temperature. The melting point of the gel (0.4 wt %) was measured using a melting point apparatus. The scanning electron microscopy (SEM) samples were prepared by drop-casting as-synthesized aggregates onto silicon wafers, followed by drying in air. SEM images were obtained using a field emission scanning electron microscope (FE-SEM). Powder X-ray diffraction (PXRD) data were collected on an X-ray diffractometer using Cu Kα radiation (λ = 1.54178 Å; 50 kV, 240 mA) at room temperature.

Rheological measurements were performed on a rheometer using a 25 mm diameter parallel plate with a 1.0 mm gap. The organogel samples were prepared by dissolving the racemate ***rac*-Δ** (1.0 wt %) directly as a solid in DCE by heating, followed by cooling the mixture to ambient temperature. Gel samples were loaded carefully onto the bottom plate. Frequency sweep experiments were conducted within the linear viscoelastic regime.

To obtain aggregates as small as possible for atomic force microscopy (AFM) characterization, the as-synthesized gel and precipitate (5 mg of ***rac*-Δ** in 1 mL of DCE or DBE) was diluted to a concentration of 0.5 g/L, spin-coated onto a mica surface at 5000 rpm, and dried in air. AFM imaging was performed immediately using the tapping mode. The cross sections and heights of individual fibers were analyzed using built-in software.

Computational Details. Density functional theory (DFT) calculations for both model dimers and both ***R*-Δ** and ***S*-Δ** were performed using Q-Chem,[66] version 4.2.0. The Perdew−Burke−Ernzerhof[67] (PBE) type of GGA exchange-correlation functional was applied for geometry optimizations with the 6-311G** basis set. The van der Waals correction was taken into account using Grimme's empirical dispersion potential.[68] The geometries of individual ***R*-Δ** and ***S*-Δ** forms as well as both *RR* and *RS* dimers were optimized in the gas phase. The binding energies for holding (i) ***R*-Δ** and ***S*-Δ** molecules together to form the *RS* dimer or (ii) two ***R*-Δ** molecules to form the *RR* dimer were calculated (Figure S3) using the energy differences between both the *RR* dimer and the *RS* dimer with their corresponding isolated monomeric triangles. The optimized coordinates of ***R*-Δ** and ***S*-Δ** as well as those for the *RS* and *RR* dimers are provided in Tables S2−S5. Structural images of individual ***R*-Δ** and ***S*-Δ** forms as well as both *RR* and *RS* dimers were produced using UCSF Chimera 1.10. Atom-to-atom distances and angles were measured (Table S1) employing Mercury 3.6.

DOI: 10.1021/acs.joc.6b00281
J. Org. Chem. 2016, 81, 2581−2588

■ ASSOCIATED CONTENT

Supporting Information

The Supporting Information is available free of charge on the ACS Publications website at DOI: 10.1021/acs.joc.6b00281.

Detailed information regarding the supporting figures and tables (PDF)

■ AUTHOR INFORMATION

Corresponding Author

*E-mail: stoddart@northwestern.edu.

Notes

The authors declare no competing financial interest.

■ ACKNOWLEDGMENTS

This article is dedicated to Professor Tien-Yau Luh on the occasion of his 70th birthday. This research is part (Project 34-944) of the Joint Center of Excellence in Integrated Nano-Systems (JCIN) at King Abdulaziz City of Science and Technology (KACST) and Northwestern University (NU). The authors thank both KACST and NU for their continued support of this research. This material is based upon work supported by National Science Foundation Grant DBI-1353682, Asian Office of Aerospace R&D Grant FA2386-13-1-4124, and the National Science Foundation under University of Pittsburgh's Grant DMB-1124131. Y. Zhou acknowledges NU for a Ryan Fellowship. Y. Zhang and G.C.S. (theory work) were supported as part of the Center for Bio-Inspired Energy Science, an Energy Frontier Research Center funded by the U.S. Department of Energy, Office of Science, Basic Energy Sciences, via Grant DE-SC0000989.

■ REFERENCES

(1) Terech, P.; Weiss, R. G. *Chem. Rev.* **1997**, *97*, 3133.
(2) Steed, J. W. *Chem. Commun.* **2011**, *47*, 1379.
(3) Steed, J. W. *Chem. Soc. Rev.* **2010**, *39*, 3686.
(4) Frederix, P. W. J. M.; Scott, G. G.; Abul-Haija, Y. M.; Kalafatovic, D.; Pappas, C. G.; Javid, N.; Hunt, N. T.; Ulijn, R. V.; Tuttle, T. *Nat. Chem.* **2014**, *7*, 30.
(5) van Esch, J. H.; Feringa, B. L. *Angew. Chem., Int. Ed.* **2000**, *39*, 2263.
(6) George, M.; Weiss, R. G. *Acc. Chem. Res.* **2006**, *39*, 489.
(7) Raeburn, J.; Zamith Cardoso, A.; Adams, D. J. *Chem. Soc. Rev.* **2013**, *42*, 5143.
(8) Raeburn, J.; Adams, D. J. *Chem. Commun.* **2015**, *51*, 5170.
(9) Fleming, S.; Ulijn, R. V. *Chem. Soc. Rev.* **2014**, *43*, 8150.
(10) Weiss, R. G. *J. Am. Chem. Soc.* **2014**, *136*, 7519.
(11) Aggeli, A.; Nyrkova, I. A.; Bell, M.; Harding, R.; Carrick, L.; McLeish, T. C. B.; Semenov, A. N.; Boden, N. *Proc. Natl. Acad. Sci. U. S. A.* **2001**, *98*, 11857.
(12) Brizard, A.; Oda, R.; Huc, I. *Top. Curr. Chem.* **2005**, *256*, 167.
(13) Edwards, W.; Smith, D. K. *J. Am. Chem. Soc.* **2014**, *136*, 1116.
(14) Jung, J. H.; Ono, Y.; Hanabusa, K.; Shinkai, S. *J. Am. Chem. Soc.* **2000**, *122*, 5008.
(15) Smith, D. K. *Chem. Soc. Rev.* **2009**, *38*, 684.
(16) Morris, K. L.; Chen, L.; Raeburn, J.; Sellick, O. R.; Cotanda, P.; Paul, A.; Griffiths, P. C.; King, S. M.; O'Reilly, R. K.; Serpell, L. C.; Adams, D. J. *Nat. Commun.* **2013**, *4*, 1480.
(17) Hasell, T.; Chong, S. Y.; Jelfs, K. E.; Adams, D. J.; Cooper, A. I. *J. Am. Chem. Soc.* **2012**, *134*, 588.
(18) Čaplar, V.; Frkanec, L.; Vujičić, N. Š.; Žinić, M. *Chem. - Eur. J.* **2010**, *16*, 3066.
(19) Makarević, J.; Jokić, M.; Raza, Z.; Štefanić, Z.; Kojić-Prodić, B.; Žinić, M. *Chem. - Eur. J.* **2003**, *9*, 5567.
(20) Watanabe, Y.; Miyasou, T.; Hayashi, M. *Org. Lett.* **2004**, *6*, 1547.
(21) Borges, A. R.; Hyacinth, M.; Lum, M.; Dingle, C. M.; Hamilton, P. L.; Chruszcz, M.; Pu, L.; Sabat, M.; Caran, K. L. *Langmuir* **2008**, *24*, 7421.
(22) Frkanec, L.; Žinić, M. *Chem. Commun.* **2010**, *46*, 522.
(23) Nagy, K. J.; Giano, M. C.; Jin, A.; Pochan, D. J.; Schneider, J. P. *J. Am. Chem. Soc.* **2011**, *133*, 14975.
(24) He, Y.; Bian, Z.; Kang, C.; Gao, L. *Chem. Commun.* **2011**, *47*, 1589.
(25) Shen, Z.; Wang, T.; Liu, M. *Langmuir* **2014**, *30*, 10772.
(26) Lin, J.; Guo, Z.; Plas, J.; Amabilino, D. B.; De Feyter, S.; Schenning, A. P. H. *Chem. Commun.* **2013**, *49*, 9320.
(27) Desiraju, G. R. *Acc. Chem. Res.* **1996**, *29*, 441.
(28) Hwang, I.; Jeon, W. S.; Kim, H.-J.; Kim, D.; Kim, H.; Selvapalam, N.; Fujita, N.; Shinkai, S.; Kim, K. *Angew. Chem., Int. Ed.* **2007**, *46*, 210.
(29) Park, D. J.; Zhang, C.; Ku, J. C.; Zhou, Y.; Schatz, G. C.; Mirkin, C. A. *Proc. Natl. Acad. Sci. U. S. A.* **2015**, *112*, 977.
(30) Kang, J.; Miyajima, D.; Mori, T.; Inoue, Y.; Itoh, Y.; Aida, T. *Science* **2015**, *347*, 646.
(31) Ajami, D.; Rebek, J. *Acc. Chem. Res.* **2013**, *46*, 990.
(32) Ajami, D.; Liu, L.; Rebek, J., Jr. *Chem. Soc. Rev.* **2015**, *44*, 490.
(33) Liu, S.; Russell, D. H.; Zinnel, N. F.; Gibb, B. C. *J. Am. Chem. Soc.* **2013**, *135*, 4314.
(34) Kumari, H.; Dennis, C. L.; Mossine, A. V.; Deakyne, C. A.; Atwood, J. L. *J. Am. Chem. Soc.* **2013**, *135*, 7110.
(35) Kumari, H.; Deakyne, C. A.; Atwood, J. L. *Acc. Chem. Res.* **2014**, *47*, 3080.
(36) Liu, Y.; Hu, C.; Comotti, A.; Ward, M. D. *Science* **2011**, *333*, 436.
(37) Beijer, F. H.; Kooijman, H.; Spek, A. L.; Sijbesma, R. P.; Meijer, E. W. *Angew. Chem., Int. Ed.* **1998**, *37*, 75.
(38) Corbin, P. S.; Zimmerman, S. C. *J. Am. Chem. Soc.* **1998**, *120*, 9710.
(39) Lafitte, V. G. H.; Aliev, A. E.; Horton, P. N.; Hursthouse, M. B.; Bala, K.; Golding, P.; Hailes, H. C. *J. Am. Chem. Soc.* **2006**, *128*, 6544.
(40) Blight, B. A.; Hunter, C. A.; Leigh, D. A.; McNab, H.; Thomson, P. I. T. *Nat. Chem.* **2011**, *3*, 246.
(41) Montenegro, J.; Ghadiri, M. R.; Granja, J. R. *Acc. Chem. Res.* **2013**, *46*, 2955.
(42) Hennig, A.; Fischer, L.; Guichard, G.; Matile, S. *J. Am. Chem. Soc.* **2009**, *131*, 16889.
(43) Fischer, L.; Decossas, M.; Briand, J.-P.; Didierjean, C.; Guichard, G. *Angew. Chem., Int. Ed.* **2009**, *48*, 1625.
(44) Pantoş, G. D.; Pengo, P.; Sanders, J. K. M. *Angew. Chem., Int. Ed.* **2007**, *46*, 194.
(45) Gong, H.-Y.; Rambo, B. M.; Karnas, E.; Lynch, V. M.; Sessler, J. L. *Nat. Chem.* **2010**, *2*, 406.
(46) Nalluri, S. K. M.; Berdugo, C.; Javid, N.; Frederix, P. W. J. M.; Ulijn, R. V. *Angew. Chem., Int. Ed.* **2014**, *53*, 5882.
(47) Ogi, S.; Stepanenko, V.; Sugiyasu, K.; Takeuchi, M.; Würthner, F. *J. Am. Chem. Soc.* **2015**, *137*, 3300.
(48) Piana, F.; Facciotti, M.; Pileio, G.; Hiscock, J. R.; Van Rossom, W.; Brown, R. C. D.; Gale, P. A. *RSC Adv.* **2015**, *5*, 12287.
(49) Kouwer, P. H. J.; Koepf, M.; Le Sage, V. A. A.; Jaspers, M.; van Buul, A. M.; Eksteen-Akeroyd, Z. H.; Woltinge, T.; Schwartz, E.; Kitto, H. J.; Hoogenboom, R.; Picken, S. J.; Nolte, R. J. M.; Mendes, E.; Rowan, A. E. *Nature* **2013**, *493*, 651.
(50) Scheiner, S. *Noncovalent Forces* **2015**, *19*, 69.
(51) Schneebeli, S. T.; Frasconi, M.; Liu, Z.; Wu, Y.; Gardner, D. M.; Strutt, N. L.; Cheng, C.; Carmieli, R.; Wasielewski, M. R.; Stoddart, J. F. *Angew. Chem., Int. Ed.* **2013**, *52*, 13100.
(52) Liu, Z.; Liu, G.; Wu, Y.; Cao, D.; Sun, J.; Schneebeli, S. T.; Nassar, M. S.; Mirkin, C. A.; Stoddart, J. F. *J. Am. Chem. Soc.* **2014**, *136*, 16651.
(53) Steiner, T. *Chem. Commun.* **1997**, 727.
(54) Kar, T.; Scheiner, S. *J. Phys. Chem. A* **2004**, *108*, 9161.
(55) Aida, T.; Meijer, E. W.; Stupp, S. I. *Science* **2012**, *335*, 813.

DOI: 10.1021/acs.joc.6b00281
J. Org. Chem. 2016, 81, 2581−2588

(56) Wu, X.; Liu, R.; Sathyamoorthy, B.; Yamato, K.; Liang, G.; Shen, L.; Ma, S.; Sukumaran, D. K.; Szyperski, T.; Fang, W.; He, L.; Chen, X.; Gong, B. *J. Am. Chem. Soc.* **2015**, *137*, 5879.
(57) Koshkakaryan, G.; Jiang, P.; Altoe, V.; Cao, D.; Klivansky, L. M.; Zhang, Y.; Chung, S.; Katan, A.; Martin, F.; Salmeron, M.; Ma, B.; Aloni, S.; Liu, Y. *Chem. Commun.* **2010**, *46*, 8579.
(58) Huang, Z.; Kang, S.-K.; Banno, M.; Yamaguchi, T.; Lee, D.; Seok, C.; Yashima, E.; Lee, M. *Science* **2012**, *337*, 1521.
(59) Yamagishi, H.; Fukino, T.; Hashizume, D.; Mori, T.; Inoue, Y.; Hikima, T.; Takata, M.; Aida, T. *J. Am. Chem. Soc.* **2015**, *137*, 7628.
(60) Ren, C.; Maurizot, V.; Zhao, H.; Shen, J.; Zhou, F.; Ong, W. Q.; Du, Z.; Zhang, K.; Su, H.; Zeng, H. *J. Am. Chem. Soc.* **2011**, *133*, 13930.
(61) Rambo, B. M.; Gong, H.-Y.; Oh, M.; Sessler, J. L. *Acc. Chem. Res.* **2012**, *45*, 1390.
(62) Meazza, L.; Foster, J. A.; Fucke, K.; Metrangolo, P.; Resnati, G.; Steed, J. W. *Nat. Chem.* **2012**, *5*, 42.
(63) Zhang, Z.; Luo, Y.; Chen, J.; Dong, S.; Yu, Y.; Ma, Z.; Huang, F. *Angew. Chem., Int. Ed.* **2011**, *50*, 1397.
(64) Steiner, T.; Desiraju, G. R. *Chem. Commun.* **1998**, 891.
(65) Gabutti, S.; Knutzen, M.; Neuburger, M.; Schull, G.; Berndt, R.; Mayor, M. *Chem. Commun.* **2008**, 2370.
(66) Shao, Y.; Gan, Z.; Epifanovsky, E.; Gilbert, A. T. B.; Wormit, M.; Kussmann, J.; Lange, A. W.; Behn, A.; Deng, J.; Feng, X.; Ghosh, D.; Goldey, M.; Horn, P. R.; Jacobson, L. D.; Kaliman, I.; Khaliullin, R. Z.; Kuś, T.; Landau, A.; Liu, J.; Proynov, E. I.; Rhee, Y. M.; Richard, R. M.; Rohrdanz, M. A.; Steele, R. P.; Sundstrom, E. J.; Woodcock, H. L.; Zimmerman, P. M.; Zuev, D.; Albrecht, B.; Alguire, E.; Austin, B.; Beran, G. J. O.; Bernard, Y. A.; Berquist, E.; Brandhorst, K.; Bravaya, K. B.; Brown, S. T.; Casanova, D.; Chang, C.-M.; Chen, Y.; Chien, S. H.; Closser, K. D.; Crittenden, D. L.; Diedenhofen, M.; DiStasio, R. A.; Do, H.; Dutoi, A. D.; Edgar, R. G.; Fatehi, S.; Fusti-Molnar, L.; Ghysels, A.; Golubeva-Zadorozhnaya, A.; Gomes, J.; Hanson-Heine, M. W. D.; Harbach, P. H. P.; Hauser, A. W.; Hohenstein, E. G.; Holden, Z. C.; Jagau, T.-C.; Ji, H.; Kaduk, B.; Khistyaev, K.; Kim, J.; Kim, J.; King, R. A.; Klunzinger, P.; Kosenkov, D.; Kowalczyk, T.; Krauter, C. M.; Lao, K. U.; Laurent, A. D.; Lawler, K. V.; Levchenko, S. V.; Lin, C. Y.; Liu, F.; Livshits, E.; Lochan, R. C.; Luenser, A.; Manohar, P.; Manzer, S. F.; Mao, S.-P.; Mardirossian, N.; Marenich, A. V.; Maurer, S. A.; Mayhall, N. J.; Neuscamman, E.; Oana, C. M.; Olivares-Amaya, R.; O'Neill, D. P.; Parkhill, J. A.; Perrine, T. M.; Peverati, R.; Prociuk, A.; Rehn, D. R.; Rosta, E.; Russ, N. J.; Sharada, S. M.; Sharma, S.; Small, D. W.; Sodt, A. *Mol. Phys.* **2014**, *113*, 184.
(67) Perdew, J. P.; Burke, K.; Ernzerhof, M. *Phys. Rev. Lett.* **1996**, *77*, 3865.
(68) Grimme, S. *J. Comput. Chem.* **2006**, *27*, 1787.

DOI: 10.1021/acs.joc.6b00281
J. Org. Chem. 2016, 81, 2581−2588